Wind-induced seismic noise at the Princess Elisabeth Antarctica Station

Baptiste FRANKINET [1,2], Thomas LECOCQ [1], Thierry CAMELBEECK [1]

[1] Royal Observatory of Belgium, Brussels, Belgium
[2] Glaciology Laboratory, Université Libre de Bruxelles, Brussels, Belgium

5   *Correspondance to Baptiste Frankinet (Baptiste.Frankinet@gmail.com)*

Abstract. Most of the icequakes recorded by the seismic station at the Belgian Princess Elisabeth Antarctica Station (PE) have small amplitudes corresponding to maximal displacements of a few nanometres. Therefore, their detection threshold is highly variable because of the rapid and strong changes in the local seismic noise level. In this study, we evaluated the influence of katabatic winds on the noise measured by the well-protected PE surface seismometer. Our purpose is to identify

10   whether the lack of icequakes detection during some periods could be associated with variations in the processes generating them or simply to a stronger seismic noise linked to stronger wind conditions. We observed that the wind mainly influences seismic noise at frequencies greater than 1 Hz. The seismic noise level well correlates linearly with the wind velocity, but this correlation follows different linear laws at wind velocity lower and greater than 6 m/s, with a respective variation of 0.4 dB/(m/s) and 1.4 dB/(m/s). These results allowed presenting a model and synthetic spectrogram that explain the

15   behaviour of the wind-induced seismic noise at PE. This model enables us partially removing the influence of wind impact from the original seismic dataset, which improves the observation of cryoseismic activity near the PE station.

1 Introduction: Icequakes

The study of icequakes provides insights into the different processes linked to ice dynamics. Icequakes, or cryoseisms, originate from the formation of crevasses, basal sliding, hydrofracturing, iceberg calving, in-glacier fracturing,

20   and glacial-seismicity triggered by an earthquake. A synthesis of the main types of icequakes and their causes is presented by Podolskiy & Walter (2016). Cryoseismic sources can have seismic signatures difficult to distinguish one from another. For example, the crevasse formation represents very short events (< 1 s) over a large frequency band (10 - 50 Hz). They have a propagation velocity of 0.01 m/s up to 30 m/s and generally do not exceed 10 μm in amplitude, that make them close in amplitude to microseismic noise or to wind-induced ground motion that can cause similar seismic signature and

25   amplitude (Bormann & Wielandt, 2013; Naderyan et al., 2016; Withers et al., 1996). Cryoseismology has not been studied thoroughly in all regions of Antarctica but thanks to the improvement of instrumentation and the increasing number of seismic stations in Antarctica, numerous studies linking seismology to glaciology have been published in the last decade. From linking the microseismicity induced by tides in the grounding line of East-Antarctica (Barruol et al., 2013), to focusing on tremors from stick-slip motions in the Whillans ice shelf (Paul Winberry et al., 2013). And from studying

30   specific cryoseismic events observed at Ekström Ice Shelf, Antarctica (Hammer et al., 2015), to observing thermal icequakes and their origins on blue ice in East-Antarctica (Lombardi et al., 2019).

1.1 The Antarctica Princess Elisabeth Belgian station and seismic stations

The Belgian Princess Elisabeth Antarctica Station (PE) was built during the first International Polar Year 2007-2008 and completed in 2008-2009. It is situated 300 m North of Usteinen nunatak (71°57' S, 23°20' E) on a small flat

35   granite ridge, a few kilometers north of the Sør Rondane mountain range. The Usteinen nunatak is approximately 700 m long and 20-30 m wide and is composed of massive coarse-grained granite with minor xenolithic blocks of metamorphic rocks (Kojima & Shiraishi, 1986). To the south, the Sør Rondane Mountains peaks have an elevation up to 4000 m and

form part of the Eastern Antarctica Precambrian shield (Pattyn et al., 1992). It allowed studying from meteorites to microbiology (Peeters et al., 2011; Pushkareva et al., 2018), glaciology (Callens et al., 2015; Frank Pattyn et al., 2010), and meteorology (clouds, aerosols, temperature) (A. Gossart et al., 2019; A. Gossart et al., 2019; Herenz et al., 2019; Souverijns et al., 2018). In parallel, the Royal Observatory of Belgium installed a permanent broadband seismic station (BE.ELIB) on the bedrock near the base in February 2010 (Camelbeeck et al., 2019). This station improves the low coverage of seismic stations in Antarctica. Indeed, the closest seismometer is located at the Novolazarevskaya base (Russia), 430 km West from PE. To the East of PE, the closest station is the Japanese Syowa site (680 km away). Because of its location, the station gave a new source of information for global seismic studies as well as for inferring the crustal structure beneath it (Camelbeeck et al., 2019). The addition of a temporary seismic network during the 2014 austral summer (see Table 1 and Figure 1) has highlighted seismic activity (see Figure 7 of Camelbeeck et al., 2019), within a radius of 150 km around the station, hitherto unknown. This seismic activity is related to the interaction between ice and bedrock or from within the ice.

1.2 Icequakes and seismic noise

Most icequakes can only be detected with seismometers while the resulting damage and movements of the ice sheet and associated glaciers can be observed by other geophysical or geodetic means, such as GPS (Capra et al., 1998) or radar interferometry (Mohr et al., 1998; Rignot et al., 2011). Cryoseismic catalogues and seismic observations can be correlated with numerical models of eastern Antarctic ice dynamics to quantify whether areas of specific activity are related to typical subglacial conditions (Lipovsky & Dunham, 2015; Nanni et al., 2020; F. Pattyn, 2010; Smith, 1997, 2006). These icequakes mostly have a very low seismic amplitude (few nanometres of displacement) but can still be detected owing to the very low seismic noise observed in Antarctica. Icequakes' signal-to-noise ratios (SNR) decrease when the noise increases, hence it is important to identify the noise sources and their power to evaluate the catalogue completeness before concluding the ice dynamics.

At PE, it exists a few anthropogenic noise sources like wind turbines, activity in the buildings, and human activities during the summer). The region is also submitted to rough meteorological conditions, composed of katabatic winds with sometimes velocities higher than 25 m/s (F. Pattyn et al., 2010). Such high-velocity winds have been known to affect the seismic data recorded (Johnson et al., 2019; Lott et al., 2017) because similarly to how tectonic earthquakes are registered by seismometers, the kinetic energy from the wind is converted into mechanical energy when it reaches the instrument enclosure which induces noise on the seismic record (Walker & Hedlin, 2010). This wind-induced seismic noise depends on wind velocity (Johnson et al., 2019). Understanding the effect of wind-induced seismic noise is crucial in monitoring icequakes as well as to understand missing icequakes in the data.

The PE and its permanent seismometer (ELIB) are relatively well protected by the mountain range from the fastest katabatic winds coming from the Antarctic Plateau. ELIB is located on the same flat granite ridge as the Princess Elisabeth Station and inside a shelter, 350 m from the base. Contrary to ELIB, the temporary seismometers installed in 2014 (Figure 1) are less protected, and more prone to wind noise. If ELIB sees an increase of seismic amplitude related to wind, the temporary seismic stations should therefore have an increased wind-induced ground motion. The base is powered by solar panels and nine Proven Energy 6kW wind turbines (WT) (Belspo, 2007). Each consists of a 9 m high tower with a 3-blade rotor that adapts the angle of the blades in relation to the wind speed to generate the maximum amount of power from low-velocity winds and reduce the amount from high-speed winds. When the wind speed is low, the angle of the three blades

is reduced up to 5° and when the wind speed is the highest, the angle can increase up to 45° which reduces by half the 5.5 m rotor diameter and the resulting rotational speed. The effect of wind turbines on seismic records has also been studied in the past and often results in noise increase in discrete frequency bands related to their shape, structure, height, the number of blades, and rotational speed (Mucciarelli et al., 2005; Stammler & Ceranna, 2016; Withers et al., 1996). Wind-induced seismic noise has energy at a wide range of frequencies (1 - 60 Hz and below 0.05 Hz), and its level decreases rapidly with depth (Withers et al., 1996). Wind-induced seismic noise characteristic frequencies and amplitudes also depend on wind interaction with man-made constructions (Hillers et al., 2015; Johnson et al., 2019; McNamara, 2004; Stammler & Ceranna, 2016). In Antarctica, with the lack of trees, the seismic noise induced by the wind should originate from the interaction with the base's buildings, wind-turbines, and topography. At longer periods, the atmospheric pressure-field can induce tilting (De Angelis & Bodin, 2012).

In this paper, we present an analysis of the influence of the wind velocity onto the seismic data from the ELIS seismometer at the Princess Elisabeth Station. By aggregating seismic data for different wind speeds, we quantify the relationship between wind energy and seismic ground motions. We present a model of the noise baseline when there is no wind and its increase for each increment of wind speed, in all frequency bands. Using this model, we compute a model of the wind-induced seismic noise for ELIB. We applied a similar model to each station of the temporary seismic network (ANT). Finally, we used these models to evaluate the impact of the wind-noise on the detectability of icequakes
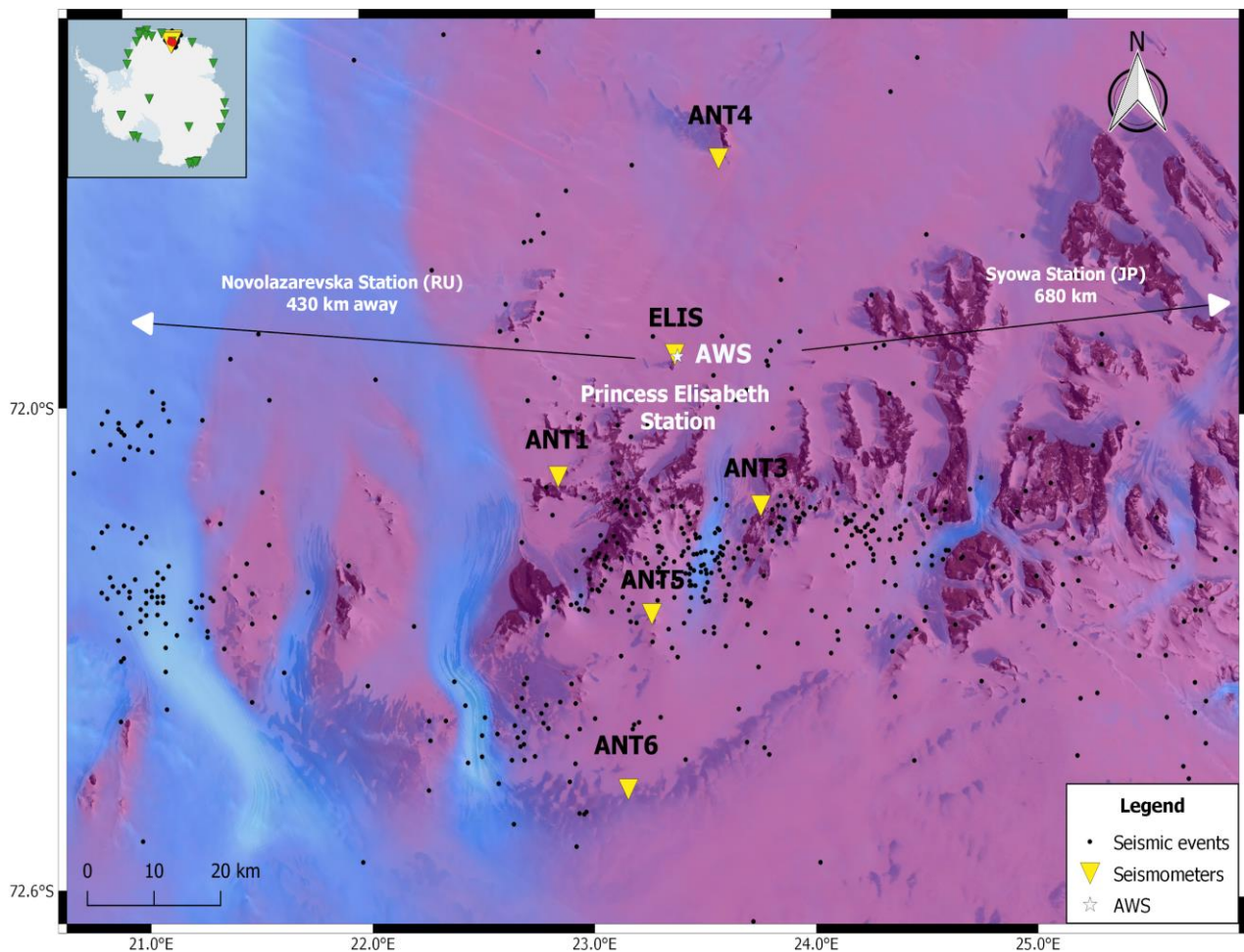
2 Data & Method

Our dataset includes seismic and wind velocity measurements at the PE base and seismic signals recorded between January and April 2014 by five temporary seismic stations, the ANT network, installed in the Sør Rondane Mountains (Figure 1).

The seismic data at the PE comes from the broadband seismic station (ELIB) installed in February 2012 (Camelbeeck et al., 2019; Lombardi et al., 2019). This station worked irregularly up to the end of 2016 due to difficulties providing continuous power supply during the austral winter, but recordings are continuous for the years 2017, 2018, and partly 2019 and 2020. The data collected by the ANT stations concern the period from January – April 2014. ELIB as well as the other temporary stations except for ANT4 use Trillium 120P, 120 s seismometers that sample at 100 samples/s, giving a recording bandwidth from 0.008 to 50 Hz, allowing to record small local seismic events as well as the worldwide large earthquakes (Camelbeeck et al., 2019). ANT4 is a Streckeisen STS-2 gen3 120 s seismometer (owned by ETH-Zurich, see Table 1).

The wind data comes from an Automated Weather Station (AWS) designed by the Institute for Marine and Atmospheric Research, Utrecht University (UU/IMAU) (van den Broeke, 2006) is provided by the AEROCLOUD project. The AEROCLOUD project aims at understanding the role of clouds and aerosols and their relation in the East Antarctic climate system The AWS is installed 300 m from the Princess Elisabeth Station, close to the ELIS seismometer site (see Figure 1 and Table 2). It has been working since February 2009 and replaced by a new AWS in December 2015, which is still in operation. The AWS is designed to work for long periods without being serviced and offers the opportunity to measure meteorological variables in remote areas and harsh weather conditions. These stations register wind speed, direction, temperature, humidity, atmospheric pressure at 2.0 m above the ground surface, and averaged over an hour window.

3

We use the seismic data from the ELIS station for the entire 2017 year (01 January 2017 - 31 December 2017), to extract hourly Power Spectral Density (PSD), which describes the power present in the signal as a function of frequency. Probabilistic PSD is then used to determine the baseline noise level (McNamara, 2004). PSDs are computed using the Obspy package (Beyreuther et al., 2010) based on the McNamara method (McNamara, 2004) which computes the PSD via a finite-range Fast Fourier Transform (FFT) of the original data (see parameters in Appendix 1). The PSDs are corrected for the instrument response to acceleration and converted to decibels (dB (m/s^2) ^{2}/Hz) to allow the comparison with the Peterson models (1993). We apply the same processing to compute the hourly PSDs for the five stations of the ANT network.

To quantify the effect of wind velocity onto the seismic data from ELIB, we aggregate the hourly PSDs for wind speeds ranging from 0.1 to 25 m/s. This provides a tool to generate synthetic PSDs for each wind speed, suppressing the wind-induced noise from the observed data.

Figure 1 : Network of instruments used in this study: 1 permanent (ELIS) and 5 temporary (ANT-) seismic stations. Other seismic stations in Antarctica reported by the International Seismograph Station Registry (http://www.isc.ac.uk/registries) are shown on the context map (green triangles) and the 2 closest from Princess Elisabeth Station are pointed towards with a white arrow: Novo. (RU) and Syowa (JP) (map was drawn with QGIS, using the Quantarctica module (Matsuoka et al., 2018)). The cryoseismic activity (Camelbeeck et al., in prep) registered by a minimum of 4 stations during the working time of the ANT network (Jan - May 2014) is shown by the small dark circles. The color scale represents the ice velocity: purple = 0 m/yr and light blue = 120 m/yr (Mouginot et al., 2019)

Station	Instrument	Location	Latitude [°]	Longitude [°]	Elevation [m]	Start	End
ELIB	Nanometrics Trillium 120P, 120 s	Princess Elisabeth Antarctica Station (borehole)	-71.947	23.346	1359	2010-02-15	2014-06-13
ELIS	Trillium 120P, 120 s	Princess Elisabeth Antarctica Station	-71.947	23.347	1372	2012-02-11	In service
ANT1	Trillium 120P, 120 s	Otto	-72.099	22.840	1718	2014-01-02	2014-04-14
ANT3	Trillium 120P, 120 s	Gunnestadbreen (outlet glacier)	-72.134	23.727	1397	2014-01-04	2014-04-14
ANT4	Streckeisen STS-2 gen3	, Vesthaugen hill (west hill)	-71.703	23.529	1217	2014-01-25	2014-08-25
ANT5	Trillium 120P, 120 s	Last Nunatak	-72.271	23.252	2366	2014-01-07	2014-03-31
ANT6	Trillium 120P, 120 s	Blue-Ice	-72.488	23.150	2379	2014-01-07	2014-12-05

Table 1: Belgian Antarctica Seismometers information.

Station	Instrument	Range +- accuracy	Direction +- Accuracy	Latitude	Longitude	Start	End
AWS	Young 05103	0 to 60 m/s +- 0.3 m/s	0 to 360° +- 3°	-71.949	23.358	2009-02-02	In service

Table 2: Automatic Weather Station (AWS) information from the AEROCLOUD Project.

3 Wind Induced Noise Model for ELIS

To quantify the link between wind velocity and seismic noise at the PE base, we computed hourly PSDs of the ELIB vertical seismometer for the whole year 2017 and extracted the 5th percentile amplitude for every 0.25 m/s wind speeds between 0 and 25 m/s (Figure 2), the maximum average wind speed recorded by the AWS which is measured at 2 m every 10 minutes interval and averaged for each hour of 2017. The 5th percentile is preferred over the average to define base noise levels for each wind speed step without taking outliers into account. The wind speed steps and their base noise amplitude exhibit (Figure 2) an increase of noise amplitude at all periods but the effect is stronger below 2 s and above 10 s. The microseism between 2 and 10 s seems less affected by the wind.
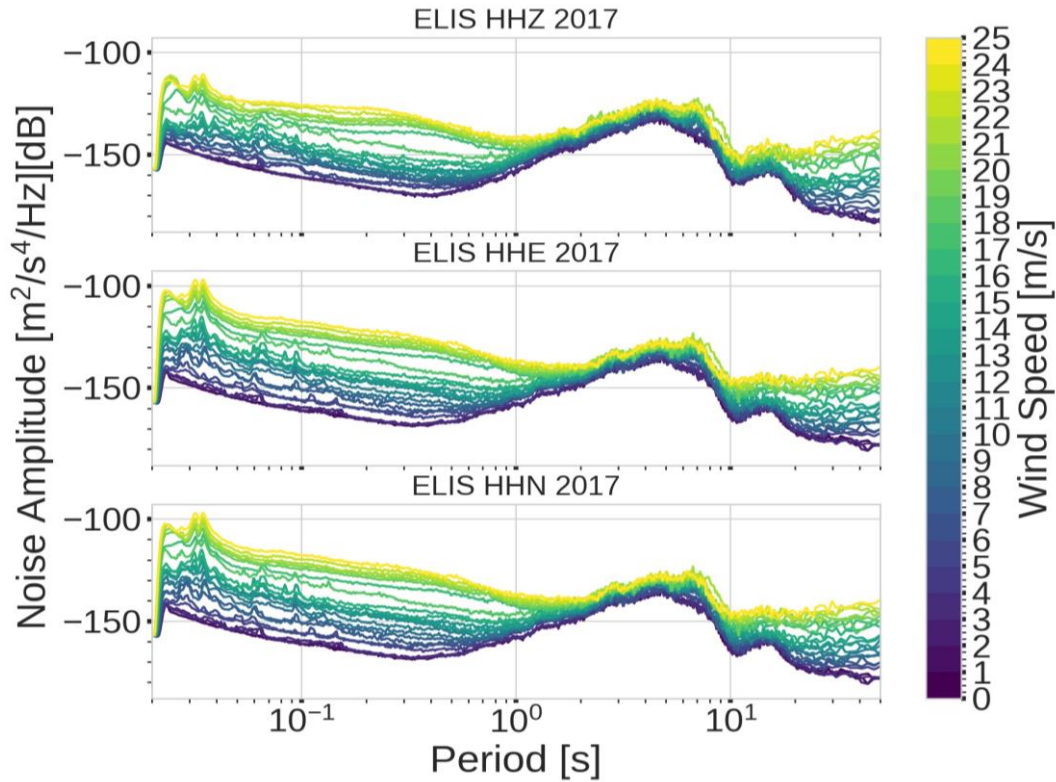
The seismic noise levels increase with the wind velocity and exhibit two different behaviour for wind velocity greater and smaller than 6 m/s. The increase of seismic noise is moderate for wind velocity from 0 to 6 m/s and larger above 6 m/s. At 0.1 s (10 Hz) there is a 42 dB difference between 0 and 25 m/s, which corresponds to a ground velocity increase of 100 times. The wind-noise effect is higher on the horizontal components than on the vertical component of the seismometer. This has been already observed and is due to the direct interaction of the wind travelling direction (horizontal) to the seismometer inducing tilt noise (Mucciarelli et al., 2005).

To create the synthetic noise model, we need to quantify seismic noise changes at each frequency with respect to the wind speed amplitude. For each period band, two linear relationships are determined between 0 and 6 m/s and above 6 m/s (slopes: a_l1 and a_l2 in Figure 3a). The data used for the weighted regression is the 5th percentile of wind speeds binned by 0.25 m/s with a minimum of 10 observations per bin. The weights are defined as the inverse of the standard deviation
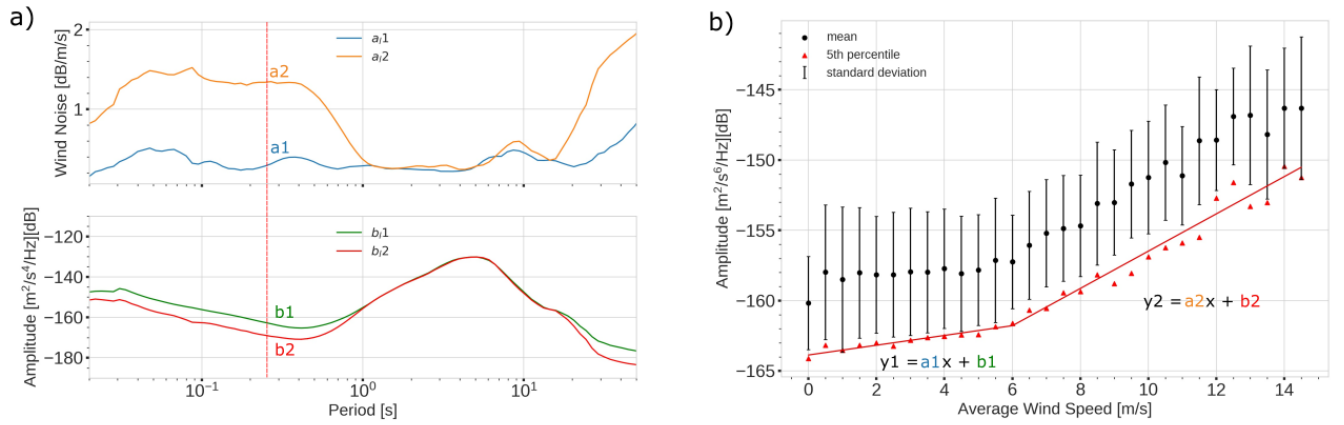
within each bin. For example, Figure 3b shows the two linear regressions at the 0.26 s period (dashed vertical line on Figure 3a): the wind-induced noise increases by approximately 2dB from 0 to 6 m/s, and after 6 dB it increases by 1.5 dB/m/s. The lower number of occurrences of wind speeds above 10 m/s could lead to instability, but the regression drawn between 6 and 10 m/s is robust and fits the observations at higher wind speed. The linear regressions are computed for every frequency and therefore describe the behaviour of the seismic noise induced by the wind at ELIS.
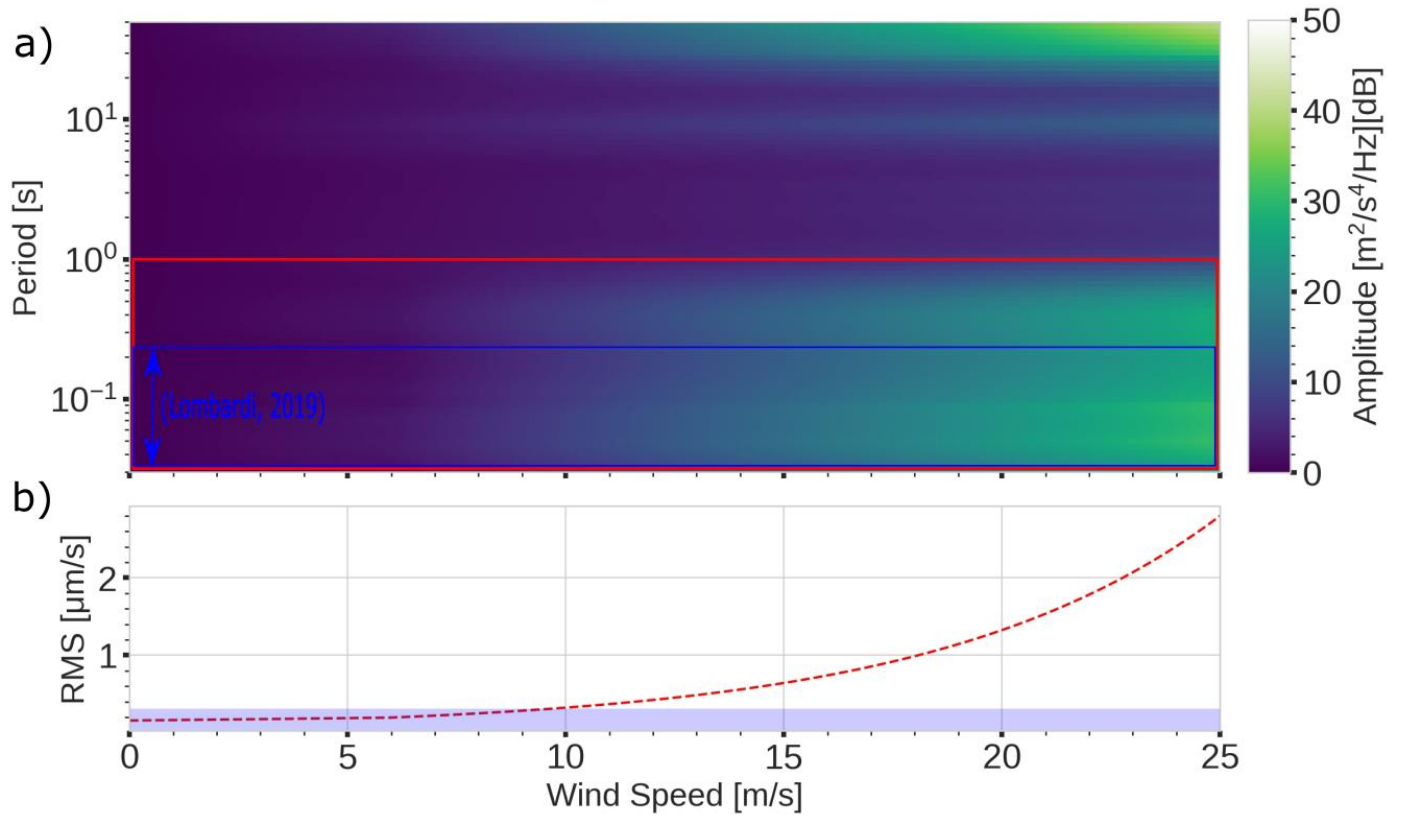
Once the linear parameters are determined for each period of the spectrum, we can run the model for any theoretical wind speed to obtain a synthetic PSD spectrum. Doing this for different wind speeds, we generate a synthetic spectrogram (Figure 4a). Transforming the synthetic PSDs to seismic velocity amplitude requires integration to PSDs of velocity and the application of Parseval's theorem that links the power spectrum and the RMS (root mean square) of a signal. The RMS velocity calculated in the 1-50 Hz frequency band (Figure 4b), i.e. the band where most cryoseismicity is expected to occur, shows an exponential increase from 0.2 to 2.8 µm/s between 0 and 25 m/s wind speed. Figure 4b also shows the frequency band (8-50 Hz) and the amplitudes (smaller than 0.3 µm) of the icequakes signals studied by Lombardi et al. (2019). This illustrates that, based on our model, Lombardi et al. (2019) have probably detected significantly fewer events when the wind speed was above 10 m/s.
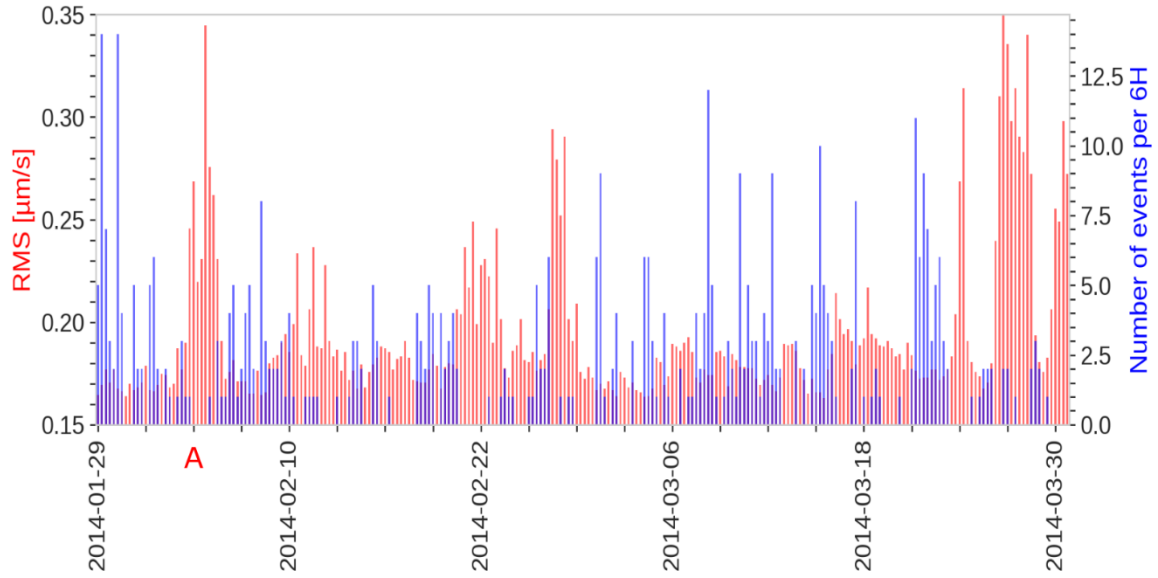

Figure 2: 2017 ELIS PSDs computed for 0 – 25 m/s wind speed

Figure 3: a): Wind Induced Noise Model describing the parameters of 2 linear functions for every period of ELIS HHZ in 2017: y = ax + b: The first subplot represents the "a" parameter and the second one the b parameter. Those 2 different linear relation parameters are until 6 m/s (a₁1/b₁1) and after 6 m/s (a₁2/b₁2). B): Behaviour of the 5ᵗʰ percentile noise amplitude for the 0.26 s period at ELIS HHZ for the average wind speed of 2017. There are 2 different linear behaviours: before 6 m/s and after 6 m/s respectively y1 and y2: the parameters used are shown on the graph a) by the red line and their parameters.

Figure 4: a) Relative Synthetic Spectrogram representing wind-induced noise increase; in blue is the frequency range of the thermal icequakes observed by Lombardi et al., 2019 and b) the 1 – 50 Hz RMS ground speed at ELIS HHZ extracted from the red rectangle on subplot a) and in light blue the amplitude range of these icequakes.

Figure 5: RMS per 6h calculated from the average wind speed and the noise model seen at ELIS vs the cumulative number of events detected per 6h (seismic rate) by Camelbeeck et al. (submitted)

3.1 Seismic Noise for the ANT network

185

We used our model to evaluate the completeness of the catalogue of icequakes identified between January and April 2014 by the ANT temporary seismic network, including ELIB station. The cumulative number of seismic events detected per 6 hours located by Camelbeeck et al. (submitted), shows an inverse correlation with the seismic noise level deduced by our model (RMS) from the wind speed measured at PE (Figure 5). This RMS is calculated from the mean wind speed registered

190 by the AWS averaged per 6h using our model shown in Figure 4b. This inverse correlation suggests that the variation in the icequakes activity rate would be directly related to seismic noise conditions induced by the wind. For example, from the 3rd to the 4th of February 2014 (A), the RMS increase from 0.17 to 0.35 µm/s at the maximum peak. The events detected over this period were affected as during the 3rd February: only 5 events were detected and, on the 4th, when the RMS increased drastically, no events were detected. We can therefore observe that a quiet station improves the detectability
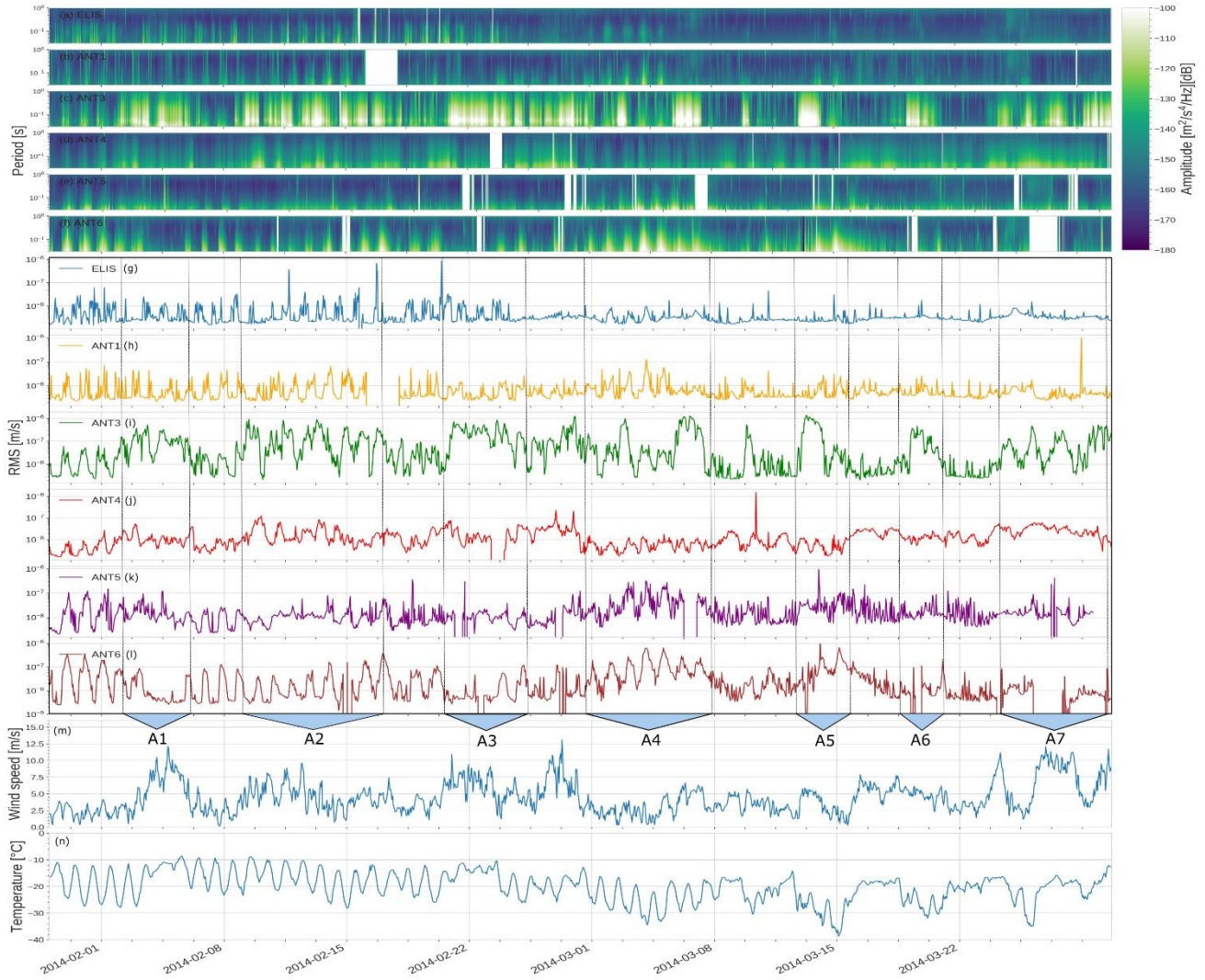
195 of icequakes.

ELIB is located in an area where the ice sheet moves very slowly, which is not the case for some of the temporary stations of the ANT network. Therefore, the ice sheet movements did not contribute greatly to the recorded seismic noise level at the ELIB seismic station. Using the 2014 data from the AWS, we can compute a synthetic seismogram for the wind-generated noise during the deployment of the temporary ANT network. Assuming that the wind field and its effects on

200 ELIS are identical at the other seismometers, which might not necessarily hold true, we obtain "clean" spectrograms by withdrawing the frequency-dependent noise increase due to wind. Figure 6a-f shows the wind-corrected spectrograms for the 6 stations, which should highlight the contribution of the cryoseismic activity of the East-Antarctic ice-sheet in the seismic noise of each station. Figure 6g-l represents the RMS velocity of the 6 previous spectrograms. For comparison, the average wind speed and temperature recorded at ELIS (Figure 6m-n) are shown.

8

The periods where the RMS velocity of the stations shows a significant cryoseismic activity are indicated by blue arrows labelled A1 to A7 (Figure 6l). Some stations, and particularly ANT3 and ANT6, still exhibit a correlation between the increase of wind speed and their remaining RMS velocity.

Between the 8 - 20 January (A1), there is a small co-increase of wind speed and RMS velocity, especially at ANT3. The same thing happens during the 8 - 15 February (A2) and 20 – 26 February (A3) intervals. 1 – 7 March (A4) shows RMS velocity peaks for all stations but ELIS, ANT1, and ANT4. The 13 – 15 March (A5) starts with a strong activity at ANT3 and then an increase in the other stations, including strong peaks at ANT6. The 18 - 20 March period (A6) as more energy on ANT3 than the other stations. The 23 – 27 February period (A7) is again dominated by strong energy at ANT3 but other stations peak during that period too (ANT6 and ANT1 particularly). The activity of ANT3 seems, in general, to be higher than on the other stations, between 1 – 28 February and after 15 March (end of A5) until the rest of the deployment.

In addition to the activity spanning over several days, the six stations show a strong diurnal activity which has been shown to be linked to temperature variation that induces thermal icequakes (Lombardi et al., 2019). Its intensity is larger at ANT6 throughout the deployment period. At all stations but especially at ELIS and ANT1, the diurnal effect seems to lessen after 8 March 2014 (A4).

Figure 6: Belgian Antarctica Network Spectrograms (1 – 50 Hz) without wind noise for the 29/01/2014 – 30/03/2014 period with their associated RMS and the average wind speed for the same period from the AWS station at ELIS.

4 Discussion

The origin of the diurnal activity could come from thermal icequakes resulting from diurnal temperature difference as observed and studied at ELIS (Lombardi et al., 2019). On all stations but especially at ANT5 and ANT6, there is a greater diurnal activity during A4 and A5, which correlates from a sudden drop of temperature and a greater temperature difference between the daytime/night-time (Figure 6). This also suggests that part of the greater activity seen at ANT3 and ANT4 is most likely caused by a greater cryoseismic activity induced by the temperature delta between the daytime/night-time. During A6 and A7, the same effect is observed, the activity greatly increased at ANT3 together with temperature deltas of about 10°C. The stronger activity diurnal activity at ANT6 can be explained by its setting: it is placed on blue ice and is, therefore, better coupled to register crevassing and thermal icequakes than the other stations on rock (Trnkoczy et al., 2012). The frequency content of this diurnal activity on ANT5 is higher frequency than on the other stations, most of the energy release is above 30 Hz.

The ANT3 station has a much higher amplitude of the seismic noise than any other station from the network. The activity at ANT3 seems to correlate with the wind for at least A1, A2, A3, and A7 periods. This indicates that to a certain extent the wind field at those stations is the same as at ELIS but that the wind strength and/or its effect on the seismic noise is

10

greater. Nevertheless, certain peaks have a high amplitude that seems hard to link to the wind activity, at least not the same wind like the one measured in ELIS. For example, to reach the peaks at 1.0 μm/s seen at ANT3, in A2, A3, and A4, the wind needs to reach a speed at least 17.5 m/s, which was not observed at ELIS during the period where the ANT network was deployed. The maximum wind speed during that period was 14 m/s. Another cause of the difference in energy could be linked to the insulation or coupling difference of the seismometer in the different stations. Part of the explanation for site-specific winds can be explained by the location of ANT3 close to an outlet glacier, which could channelize the winds originating from the Plateau to the south.

The continuously higher energy at ANT4 follows the same general long-term trends as the wind speed. There seems therefore to be a small under-correction of the wind effect on the noise, caused either by slightly stronger local winds, or a slightly steeper relationship between wind and noise caused by coupling or installation settings. Stronger continuous cryoseismic activity could also explain the observations but based on Lombardi et al. (2019) we would expect to see more diurnal variation if this activity was thermally induced.

From the stations in the network, ANT1, ANT3, and ANT5 are the closest to the a priori more seismogenic zones: the collision between the glaciers and the mountains and the zone of channelized glaciers with greater ice flow speed (Figure 1).

5 Conclusions

Near the Princess Elisabeth Station, we observe a wind-induced seismic noise that in some cases surpasses the detectability of most icequakes. The detection of icequakes can be altered by wind speed as low as 5 m/s, as they will be hidden in the wind-induced noise. When these winds reach their highest speeds, of up to 25 m/s, the seismometer registers an increase of 100 times the seismic velocity of a stand-still moment (0.5 μm/s to 3 μm/s) making most of the small icequakes undetectable. Understanding the effect of wind-induced seismic noise is therefore crucial in monitoring icequakes as well as to understand missing icequakes in the data.

Using the data from the permanent seismic station ELIS, we provide a synthetic model that simulates the ground motion spectrum for different wind speeds. For half of the period during which the temporary ANT network was deployed, the ANT3 seismometer exhibits greater amplitude than the other stations which can only be partially explained by greater local wind speeds. After correcting the seismograms for wind-induced noise and computing the RMS velocity, we found that some peaks still follow the wind speed in some cases but most of the time it stays independent from it.

As observed elsewhere, we suggest that the diurnal changes of energy observed are linked to cycles of cryoseismic activity induced by the large diurnal temperature delta between the daytime/night-time. The longer-lasting energy releases, on the other hand, could have different causes related or not to wind. They could either originate from slightly different wind fields, wind speeds, or couplings; or from an increased cryoseismic activity occurring in the vicinity of the station, independently from the diurnal and thermal effects, for example, crevasses or basal stick-slip events. The diurnal seismic energy at a higher frequency on ANT5 could result from different source mechanisms, with smaller, shorter icequakes occurring in the direct vicinity of the station. This could be confirmed by studying and comparing the icequakes signatures on the different stations in future work.

11

6 Acknowledgments

7 References

Barruol, G., Cordier, E., Bascou, J., Fontaine, F. R., Legrésy, B., & Lescarmontier, L. (2013). Tide-induced microseismicity in the Mertz glacier grounding area, East Antarctica: MERTZ GLACIER TIDE-MODULATED ICEQUAKES. *Geophysical Research Letters*, *40*(20), 5412–5416. https://doi.org/10.1002/2013GL057814

Belspo. (2007, March). Construction and operation of the new Belgian Research Station, Dronning Maud Land, Antarctica: FINAL COMPREHENSIVE ENVIRONMENTAL EVALUATION REPORT (CEE).

Beyreuther, M., Barsch, R., Krischer, L., Megies, T., Behr, Y., & Wassermann, J. (2010). ObsPy: A Python Toolbox for Seismology. *Seismological Research Letters*, *81*(3), 530–533. https://doi.org/10.1785/gssrl.81.3.530

Bormann, P., & Wielandt, E. (2013). Seismic Signals and Noise. *New Manual of Seismological Observatory Practice 2 (NMSOP2)*, 62.

van den Broeke, Prof. M. R. (2006). Automatic weather stations in interior East Antarctica.

Callens, D., Thonnard, N., Lenaerts, J. T. M., Van Wessem, J. M., Van de Berg, W. J., Matsuoka, K., & Pattyn, F. (2015). Mass balance of the Sør Rondane glacial system, East Antarctica. *Annals of Glaciology*, *56*(70), 63–69. https://doi.org/10.3189/2015AoG70A010

Camelbeeck, T., Lombardi, D., Collin, F., Rapagnani, G., Martin, H., & Lecocq, T. (2019). Contribution of the seismic monitoring at the Belgian Princess Elisabeth base to East Antarctica ice sheet dynamics and global seismicity studies. *Bulletin Des Séances- Académie Royale Des Sciences d'outre-Mer*, *63*.

Capra, A., Frezzotti, M., Mancini, F., Radicioni, F., & Vittuari, L. (1998). GPS for ice sheet movement monitoring and grounding line detection. In R. Forsberg, M. Feissel, & R. Dietrich (Eds.), *Geodesy on the Move* (Vol. 119, pp. 486–491). Berlin, Heidelberg: Springer Berlin Heidelberg. https://doi.org/10.1007/978-3-642-72245-5_82

De Angelis, S., & Bodin, P. (2012). Watching the Wind: Seismic Data Contamination at Long Periods due to Atmospheric Pressure-Field-Induced Tilting. *Bulletin of the Seismological Society of America*, *102*(3), 1255–1265. https://doi.org/10.1785/0120110186

Gossart, A., Helsen, S., Lenaerts, J. T. M., Broucke, S. V., van Lipzig, N. P. M., & Souverijns, N. (2019). An Evaluation of Surface Climatology in State-of-the-Art Reanalyses over the Antarctic Ice Sheet. *Journal of Climate*, *32*(20), 6899–6915. https://doi.org/10.1175/JCLI-D-19-0030.1

Gossart, Alexandra, Palm, S. P., Souverijns, N., Lenaerts, J. T. M., Gorodetskaya, I. V., Lhermitte, S., & van Lipzig, N. P. M. (2019). Blowing snow in East Antarctica: comparison of ground-based and space-borne retrievals. *The Cryosphere Discussions*, 1–19. https://doi.org/10.5194/tc-2019-25

Hammer, C., Ohrnberger, M., & Schlindwein, V. (2015). Pattern of cryospheric seismic events observed at Ekström Ice Shelf, Antarctica. *Geophysical Research Letters*, *42*(10), 3936–3943. https://doi.org/10.1002/2015GL064029

Herenz, P., Wex, H., Mangold, A., Laffineur, Q., Gorodetskaya, I. V., Fleming, Z. L., et al. (2019). CCN measurements at the Princess Elisabeth Antarctica research station during three austral summers. *Atmospheric Chemistry and Physics*, *19*(1), 275–294. https://doi.org/10.5194/acp-19-275-2019

Hillers, G., Ben-Zion, Y., Campillo, M., & Zigone, D. (2015). Seasonal variations of seismic velocities in the San Jacinto fault area observed with ambient seismic noise. *Geophysical Journal International*, *202*(2), 920–932. https://doi.org/10.1093/gji/ggv151

Johnson, C. W., Meng, H., Vernon, F., & Ben-Zion, Y. (2019). Characteristics of Ground Motion Generated by Wind Interaction With Trees, Structures, and Other Surface Obstacles. *Journal of Geophysical Research: Solid Earth*, 2018JB017151. https://doi.org/10.1029/2018JB017151

Kojima S., & Shiraishi K. (1986). Note on the geology of the western part of the Soer Rondane Mountains, East Antarctica, *43*, 116–131.

Lipovsky, B. P., & Dunham, E. M. (2015). Tremor during ice stream stick-slip. *The Cryosphere Discussions*, *9*(5), 5253–5289. https://doi.org/10.5194/tcd-9-5253-2015

Lombardi, D., Gorodetskaya, I., Barruol, G., & Camelbeeck, T. (2019). Thermally induced icequakes detected on blue ice areas of the East Antarctic ice sheet. *Annals of Glaciology*, 1–12. https://doi.org/10.1017/aog.2019.26

Lott, F. F., Ritter, J. R. R., Al-Qaryouti, M., & Corsmeier, U. (2017). On the Analysis of Wind-Induced Noise in Seismological Recordings: Approaches to Present Wind-Induced Noise as a Function of Wind Speed and Wind Direction. *Pure and Applied Geophysics*, *174*(3), 1453–1470. https://doi.org/10.1007/s00024-017-1477-2

McNamara, D. E. (2004). Ambient Noise Levels in the Continental United States. *Bulletin of the Seismological Society of America*, *94*(4), 1517–1527. https://doi.org/10.1785/012003001

Mohr, J. J., Reeh, N., & Madsen, S. N. (1998). Three-dimensional glacial flow and surface elevation measured with radar interferometry. *Nature*, *391*(6664), 273–276. https://doi.org/10.1038/34635

Mucciarelli, M., Gallipoli, M. R., Di Giacomo, D., Di Nota, F., & Nino, E. (2005). The influence of wind on measurements of seismic noise. *Geophysical Journal International*, *161*(2), 303–308. https://doi.org/10.1111/j.1365-246X.2004.02561.x

13

Naderyan, V., Hickey, C. J., & Raspet, R. (2016). Wind-induced ground motion. *Journal of Geophysical Research: Solid Earth*, *121*(2), 917–930. https://doi.org/10.1002/2015JB012478

Nanni, U., Gimbert, F., Vincent, C., Gräff, D., Walter, F., Piard, L., & Moreau, L. (2020). Quantification of seasonal and diurnal dynamics of subglacial channels using seismic observations on an Alpine glacier. *The Cryosphere*, *14*(5), 1475–1496. https://doi.org/10.5194/tc-14-1475-2020

Pattyn, F., Decleir, H., & Huybrechts, P. (1992). Glaciation of the central part of the Soer Rondane, Antarctica: glaciological evidence. *In: Yoshida, Y. et al. (Eds): Recent Progress in Antarctic Earth Science, Terrapub (Tokyo)*, 669–678.

Pattyn, Frank. (2010). Antarctic subglacial conditions inferred from a hybrid ice sheet/ice stream model. *Earth and Planetary Science Letters*, *295*(3–4), 451–461. https://doi.org/10.1016/j.epsl.2010.04.025

Pattyn, Frank, Matsuoka, K., & Berte, J. (2010). Glacio-meteorological conditions in the vicinity of the Belgian Princess Elisabeth Station, Antarctica. *Antarctic Science*, *22*(01), 79. https://doi.org/10.1017/S0954102009990344

Paul Winberry, J., Anandakrishnan, S., Wiens, D. A., & Alley, R. B. (2013). Nucleation and seismic tremor associated with the glacial earthquakes of Whillans Ice Stream, Antarctica: GLACIAL SEISMIC TREMOR. *Geophysical Research Letters*, *40*(2), 312–315. https://doi.org/10.1002/grl.50130

Peeters, K., Ertz, D., & Willems, A. (2011). Culturable bacterial diversity at the Princess Elisabeth Station (Utsteinen, Sør Rondane Mountains, East Antarctica) harbours many new taxa. *Systematic and Applied Microbiology*, *34*(5), 360–367. https://doi.org/10.1016/j.syapm.2011.02.002

Peterson, J. (1993). *Observations and modeling of seismic background noise* (Open-File Report).

Podolskiy, E. A., & Walter, F. (2016). Cryoseismology: CRYOSEISMOLOGY. *Reviews of Geophysics*, *54*(4), 708–758. https://doi.org/10.1002/2016RG000526

Pushkareva, E., Pessi, I. S., Namsaraev, Z., Mano, M.-J., Elster, J., & Wilmotte, A. (2018). Cyanobacteria inhabiting biological soil crusts of a polar desert: Sør Rondane Mountains, Antarctica. *Systematic and Applied Microbiology*, *41*(4), 363–373. https://doi.org/10.1016/j.syapm.2018.01.006

Rignot, E., Mouginot, J., & Scheuchl, B. (2011). Ice Flow of the Antarctic Ice Sheet. *Science*, *333*(6048), 1427–1430. https://doi.org/10.1126/science.1208336

Smith, A. M. (1997). Basal conditions on Rutford Ice Stream, West Antarctica, from seismic observations. *Journal of Geophysical Research: Solid Earth*, *102*(B1), 543–552. https://doi.org/10.1029/96JB02933

Smith, A. M. (2006). Microearthquakes and subglacial conditions. *Geophysical Research Letters*, *33*(24), L24501. https://doi.org/10.1029/2006GL028207

Souverijns, N., Gossart, A., Gorodetskaya, I. V., Lhermitte, S., Mangold, A., Laffineur, Q., et al. (2018). How does the ice sheet surface mass balance relate to snowfall? Insights from a ground-based precipitation radar in East Antarctica. *The Cryosphere*, *12*(6), 1987–2003. https://doi.org/10.5194/tc-12-1987-2018

Stammler, K., & Ceranna, L. (2016). Influence of Wind Turbines on Seismic Records of the Gräfenberg Array. *Seismological Research Letters*, *87*(5), 1075–1081. https://doi.org/10.1785/0220160049

Walker, K. T., & Hedlin, M. A. H. (2010). A Review of Wind-Noise Reduction Methodologies. In A. Le Pichon, E. Blanc, & A. Hauchecorne (Eds.), *Infrasound Monitoring for Atmospheric Studies* (pp. 141–182). Dordrecht: Springer Netherlands. https://doi.org/10.1007/978-1-4020-9508-5_5

Withers, M. M., Aster, R. C., Young, C. J., & Chael, E. P. (1996). High-Frequency Analysis of Seismic Background Noise as a Function of Wind Speed and Shallow Depth, 9.

365

370

375

380

385

Appendix 1

PSD parameters: we <u>binned</u> PSDs for every hour-segment of the entire year. Parameters such as a 3600 s time window length were used for the PSD computation, which shows that long time seismic series are required to compute significant PSD plots <u>and also correspond to the wind data of the AWS station we will compare it to</u>. We did not overlap the time series to have exact PSDs estimates for each hour. Other parameters, such as "period_smoothing_width_octaves = 0.025" means that the PSD is averaged over 1/40 of an octave at each central frequency/period. We limited our computations to 50 Hz which is known as the Nyquist frequency of the seismometers. Those parameters are important to identify ~~noise~~ characteristics buried in the noise such as weak seismic peaks to differentiate each PSD with more details.

Power Spectral Density parameters calculations:

tr.stats, metadata=sp,

ppsd_length=3600, overlap=0.0,

period_smoothing_width_octaves=0.025,

period_step_octaves=0.0125,

period_limits=(0.02, 50),

db_bins=(-200, 20, 0.5)